

https://doi.org/10.1038/s43247-024-01604-3

Electrodeposition of calcareous cement from seawater in marine silica sands

Check for updates

The erosion of marine sediments is a pressing issue for coastal areas worldwide. Established methods to mitigate coastal erosion fail to provide lasting and sustainable solutions to protect marine ecosystems. Here we demonstrate the application of mild electrical stimulations to precipitate calcareous mineral binders from seawater in the pores of marine soils via electrodeposition, an alternative approach to mitigating coastal erosion. Results of electrochemical laboratory experiments unveil that the polymorphs, precipitation sites, intrusion mechanisms, and effects of electrodeposited minerals in marine sands vary as a function of the magnitude and duration of applied voltage, soil relative density, and electrolyte ionic concentration. Surprisingly, in addition to the precipitation of calcium carbonate and magnesium hydroxide, the formation of hydromagnesite is also observed due to electrically driven fluctuations in the local *pH*. These electrodeposits lead to enhanced mechanical and hydraulic properties of the marine sands, indicating that electrodeposition routes could be developed to reinforce marine soils in coastal areas that more closely mimic natural systems.

Coastal areas support the world's most heavily developed regions¹ and house approximately 40% of the global population². Yet, coastal areas face daunting challenges in the wake of extreme weather and rising sea-level, particularly erosion^{1,3,4}.

Conventional methods to mitigate coastal erosion include seawalls^{4,5} and beach replenishment^{6,7}. However, these approaches are effective only within timeframes of a few years, representing costly and temporary solutions that require recursive retrofit⁸. In contrast, natural systems, such as coral reefs^{7,9} and ecological barriers^{7,10,11}, not only enhance coastal resilience, but also provide more structural support and can even contribute to beach accretion⁸.

Inspired by the way marine organisms utilize metabolic energy to grow their skeletons and shells through mineral precipitations in seawater, capable of resisting even the most extreme perturbations, this work explores an emerging and potentially disruptive approach to mitigate the erosion of marine soils. This approach consists of using electrical energy to precipitate comparable mineral precipitations to those that build the skeletons and shells of marine organisms in the pores of marine soils for cementation purposes and the ultimate enhancement of the erosion resistance of such materials.

The possibility to precipitate solid mineral binders in seawater through the application of mild electrical stimulations derives from the large buffering capacity^{12,13} and wide availability of ions^{14,15} characterizing such an electrolyte, and the process of electrodeposition¹⁶: the electrically mediated precipitation of minerals dissolved in solutions. Specifically, when an

electrical current is applied to seawater, a variety of reduction and oxidation (redox) reactions occur, along with solid precipitations ¹⁷. These reactions commence with the release of hydroxide ions (OH^-) around cathodic interfaces, leading to an increase in the local pH. Under these conditions, the generated hydroxide ions react with naturally dissolved divalent cations in seawater $(Mg^{2+}$ and $Ca^{2+})$ and bicarbonate anions (HCO_3^-) , yielding the otherwise non-spontaneous precipitation of two ubiquitous minerals: magnesium hydroxide $(Mg(OH)_2)$ and calcium carbonate $(CaCO_3)^{18,19}$.

Currently, the electrodeposition of minerals in seawater is largely exploited to protect marine structures against corrosion^{20–22}, contribute to marine life^{16,23,24}, and heal cracks in shoreside infrastructure^{25,26}. Recent experimental evidence shows that electrodeposition can also cement marine substrates in contact with metallic structures²⁷ and the minerals formed in this manner appear to be durable²⁸. However, the understanding of the influence of electrodeposition on the structure and properties of marine soils remains limited. In this context, a knowledge gap exists due to the apparent absence of studies examining the influence of the magnitude of the applied voltage on mineral selectivity, composition, spatial distribution, intrusion mechanisms, and effects on soil properties, despite voltage being the driver of electrodeposition. Although a mechanistic understanding of the reactions and products of electrodeposition has been achieved for seawater¹⁷, this knowledge is unavailable for soils, where the electrical and kinetic phenomena ruling electrodeposition are inherently more complex due to the influence of geometric, physical, and chemical constraints exerted by the

¹Department of Civil and Environmental Engineering, Subsurface Opportunities and Innovations Laboratory, Northwestern University, 2145 Sheridan Road, Evanston, IL, 60208, USA. ²Department of Earth and Planetary Sciences, Northwestern University, 2145 Sheridan Road, Evanston, IL, 60208, USA. ²Department of Earth and Planetary Sciences, Northwestern University, 2145 Sheridan Road, Evanston, IL, 60208, USA. ³Department of Earth and Planetary Sciences, Northwestern University, 2145 Sheridan Road, Evanston, IL, 60208, USA.

pore network of such materials. Therefore, the implications of variable reaction regimes and mineral formations that can be achieved with different electrochemical potentials on the structure and properties of marine soils remain uncharted.

The fundamental hypothesis of this work is that the electrodeposition in marine soils depends principally on the features of the (1) electrical treatment, (2) soil fabric, and (3) electrolyte solution. To test this overarching hypothesis, we carried out two distinct types of experiments in custom-designed electrochemical cells on silica sand under highly controlled conditions (see Methods). The first involved short-term batch experiments with no water recirculation to uncover the selectivity of electrodeposits in soils. The second comprised long-term experiments with periodic water recirculation to unveil the intrusion mechanisms and effects of electrodeposits in soils under conditions comparable to open seawater environments. Altogether, these experiments explored the influence of the following central variables for the features of applied electrical treatments, treated porous materials, and electrolyte solutions: (1) magnitude and duration of the applied voltage, (2) soil relative density, and (3) electrolyte ionic concentration, respectively. Multiple physical, chemical, and mechanical characterization methods were used to investigate the morphology, structure, composition, spatial distribution, and effects of electrodeposited minerals in sand.

The results of this work uncover key mechanisms and effects of the artificial precipitation of minerals in marine soils, advancing geochemical knowledge and supporting engineering and technology in the development of more effective mitigation strategies for coastal erosion.

Results

Physical characterization

Physical characterization achieved via scanning electron microscopy (SEM), Raman spectroscopy, and imaging analyses of the electrodeposited minerals highlights key microscopic features of their precipitation loci, morphology, and polymorphism, along with apparent macroscopic effects on the silica sand (Fig. 1, Methods). The first uncovered pattern is that the precipitation loci and type of electrodeposits depend on the applied voltage, which governs the reaction regimes and hence the electrodeposition process (Fig. 1a). At a relatively low voltage (2.0 V), sparse electrodeposits surround sand particles without significantly bonding them together (Fig. 1a, row 1, column 1). At a medium voltage (3.0 V) and high voltage (4.0 V), denser electrodeposits surround and bond sand particles via mineral bridges (Fig. 1a, row 1, columns 2 and 3). The SEM results consistently indicate two dominant mineral formations: CaCO3 in the forms of calcite (rhombohedral morphology) and aragonite (needle-like morphology)29, as well as $Mg(OH)_2$ in the form of brucite (fibrous compounds constituted of lamellar structures)^{18,19}. CaCO₃ formations appear especially at lower voltages (Fig. 1a, rows 2 and 3, columns 1 and 2), whereas $Mg(OH)_2$ formations are mainly electrodeposited at higher voltages (Fig. 1a, rows 2 and 3, column 3); when both $CaCO_3$ and $Mg(OH)_2$ are electrodeposited, $Mg(OH)_2$ minerals coat the silica soil particles and form a substrate for the precipitation of CaCO₃ minerals (Fig. 1a, rows 2 and 3).

An analysis of SEM images of selected samples of the tested silica sand shows that $Mg(OH)_2$ is formed as both lamellar and block brucite, and $CaCO_3$ is found in the increasingly stable forms of vaterite, aragonite, and calcite (with aragonite dominating in quantity with respect to calcite and vaterite) (Fig. 1b). Notably, a quantitative analysis of Raman spectra of precipitated minerals on the silica sands consistently indicates $CaCO_3$ precipitations in the forms of calcite and aragonite, as well as $Mg(OH)_2$ in the form of brucite; additionally, Raman spectra also unveil the precipitation of hydromagnesite, $Mg_5(CO_3)_4(OH)_2 \cdot 4H_2O$ (Fig. 1c and Supplementary Fig. 1). XRD analyses reported in the sequel (Fig. 2e) also quantitatively confirm such evidence.

A second discernible pattern in the electrodeposition of minerals in marine sands is that the size and precipitation loci of electrodeposits depend on the relative density (Fig. 1d), which is a proxy of porosity. Loose sands exhibit smaller minerals and more uniform and widespread precipitations (Fig. 1d, columns 1 and 2). In contrast, dense sands exhibit larger minerals and less uniform and widespread precipitations, as well as more aragonite compared with calcite, with almost no brucite (Fig. 1d, columns 3 and 4).

An analysis of the volume and mass of "cemented" (or affected) sand elucidates a third discernible feature for the electrodeposition in marine soils (Fig. 1e); the volume of soils influenced by electrodeposits depends on the duration and magnitude of the applied electrical stimulation. After 7 days of treatment, a limited volume of sand is cemented by electrodeposits. The largest cemented volume is achieved for 3.0 V, whereas smaller volumes are achieved (in order) for 4.0 and 2.0 V. After 28 days, a larger volume of sand is cemented by electrodeposits. The largest cemented volume is achieved for 4.0 V, whereas smaller volumes are achieved (in order) for 3.0 and 2.0 V. For a given voltage, the affected volume of electrodeposits decreases with an increase in the soil relative density, whereas it increases for a longer electrical stimulation. Extending the duration of the electrical stimulation from 7 to 28 days does not significantly change the extent of the cemented volume of sand for 2.0 and 3.0 V, whereas it tremendously enhances such extent for 4.0 V. After 7 days, the soil area affected by electrodeposition reaches a radial distance of about 2-3 times the electrode diameter for 3.0 V. In contrast, this area exceeds a radial distance of 20 times the electrode diameter after 28 days of treatment with 4.0 V.

Consideration of the macroscopic effects of electrodeposition for varying magnitudes of voltage elucidates a final feature for the electrodeposition of minerals in marine soils (Fig. 1f); there exist distinct intrusion mechanisms and extents of volumes affected by electrodeposition, mainly as a function of changes in the electrochemical reactions ruling electrodeposition (see Discussion and Supplementary Discussion). The application of a low voltage (2.0 V) over a prolonged time yields electrodeposits near the cathode, which penetrate in the soil farther away from the electrode for a medium voltage (3.0 V) and influence a significant portion of the bulk of the soil for a high voltage (4.0 V). Comparable results are obtained within shorter timeframes (Supplementary Fig. 2), with the difference that the overall volume influenced by electrodeposits is consistently less significant. As electrodeposits grow within sands, they form a cemented material. Electrical current and resistance vary according to such mineral formations, with an overall decrease of the former and an increase of the latter due to the constant applied potential over time (Supplementary Fig. 3).

Chemical characterization

Chemical characterization of the environmental conditions in the sand and the electrodeposits (Fig. 2) achieved by pH measurements, energy dispersive X-ray spectroscopy (EDS), X-ray diffraction (XRD), and thermogravimetric analyses (TGA) (see Methods) supports an enhanced analysis of the mineral properties and their formation in closed and open electrochemical systems. The temporal variations of pH at the anode (Fig. 2a) and cathode (Fig. 2b) measured in the short-term in a closed system show that the pH in the sand can change significantly, leading to the creation of an acidic environment near the anode and a more alkaline environment near the cathode due the influence of oxidation and reduction reactions, respectively. For both loose and dense sands, the low voltage level (i.e., 2.0 V) results in minimal to negligible changes in pH. However, for the highest voltage level (i.e., 4.0 V) the impact is considerable. In all cases, pH variations are delayed in dense sands due to their smaller porosity and greater tortuosity compared to loose sands. Upon the termination of the electrical conditioning, the pH starts to return to its initial value. In contrast, the temporal variations of pH at the anode and cathode (Fig. 2c) measured in the long-term tests in an open system highlight minimal to negligible variations in pH due to the periodic recirculation of seawater. By refilling the system with Ca^{2+} and Mg^{2+} ions, these conditions keep the bulk electrolyte ionic concentration approximately constant.

An analysis of the elemental mapping obtained via EDS for loose and dense sands (Fig. 2d and Supplementary Fig. 4) reveals a decrease in the Ca/Mg ratio with increasing voltage, consistently with all the qualitative results obtained via SEM (Fig. 1a). The same trend for the Ca/Mg ratio as a function of the applied voltage is calculated from the Rietveld refinement of

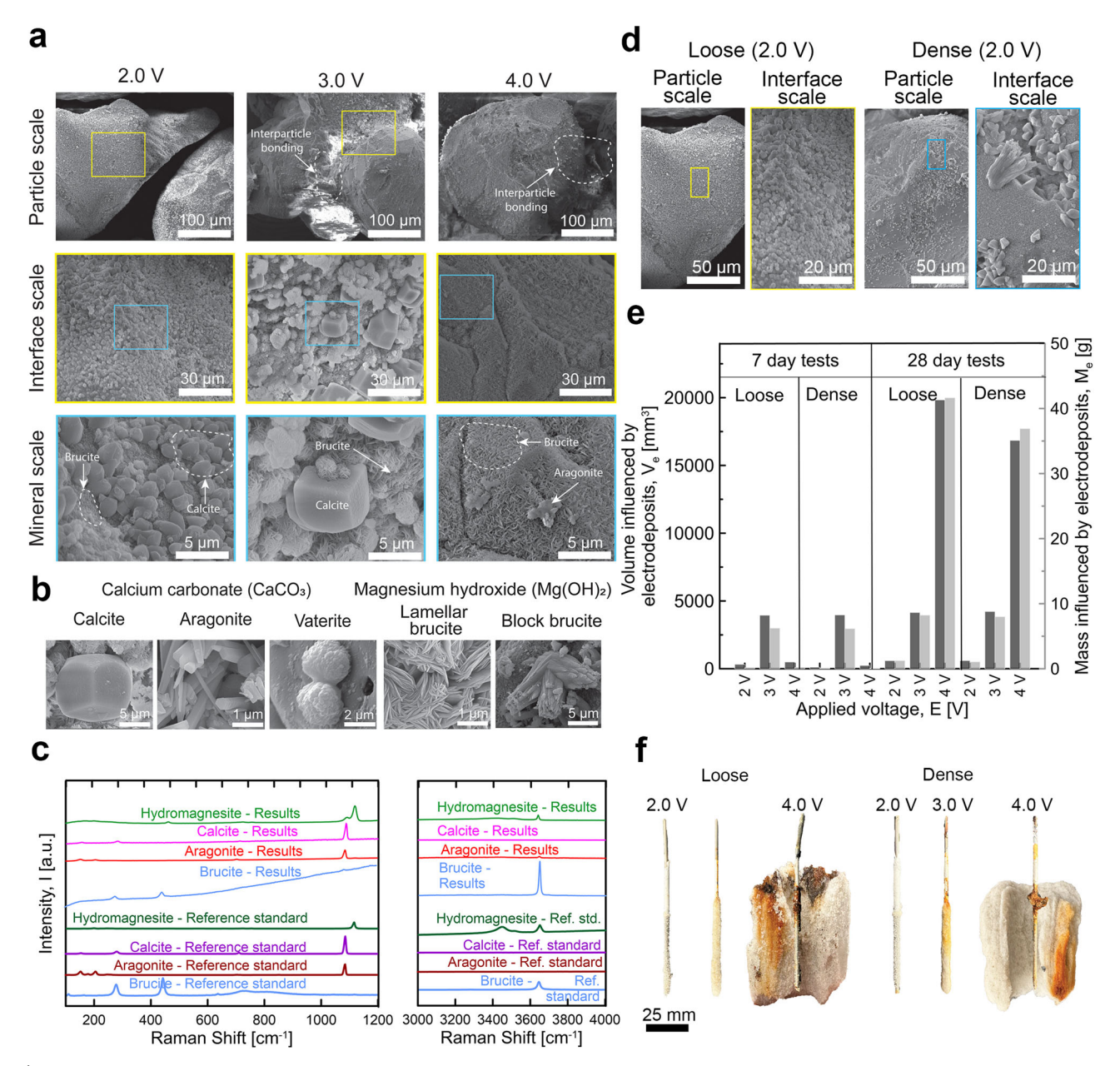


Fig. 1 | Influence of selective electrodeposition on the structure of silica sand. a SEM images at different scales (i.e., particle, interface, and mineral scale) of loose silica sand subjected to short-term electrical conditioning (i.e., 7 days) at voltages of 2.0, 3.0, and 4.0 V; b SEM images of all the visible solid minerals achieved by electrodeposition; c Raman spectra for minerals precipitated in the tested sands, compared with reference

spectra; \mathbf{d} SEM images on silica sand at different relative densities (i.e., loose and dense) at a voltage of 2.0 V; \mathbf{e} Summary of the affected volumes of cemented (or affected) sand at voltages of 2.0, 3.0, and 4.0 V for short-term tests (7 days) and long-term tests (28 days); \mathbf{f} Photographs of the effects of the distinct intrusion mechanisms associated with variable voltages for the long-term tests at 2.0, 3.0, and 4.0 V.

the XRD spectra (Fig. 2e and Supplementary Fig. 5) and the TGA results (Fig. 2f and Supplementary Fig. 6). The quantitative differences between the obtained trends for the Ca/Mg ratio are associated with the different techniques employed to analyze this variable, remaining qualitatively consistent. Notably, both the XRD and TGA results confirm again the dominant precipitation of calcium-based minerals at limited voltages, as opposed to the dominant precipitation of magnesium-based minerals at substantial voltages, as previously shown by the SEM analyses (Fig. 1a). The XRD analyses substantiate the presence of vaterite, calcite, aragonite, brucite, and hydromagnesite, as previously highlighted by the Raman spectra (Fig. 1c and Supplementary Fig. 1).

Hydromechanical characterization

The nucleation and growth of mineral electrodeposits change the structure of marine sands. Consequently, these mineral precipitations

modify the properties of such materials. The results of this work quantitatively unveil changes in the hydraulic conductivity, k, and the unconfined compressive strength, UCS, of marine sands subjected to electrodeposition (Fig. 3).

A hydraulic characterization of the sands subjected to long-term electrical conditioning (Fig. 3a) indicates a decreasing trend in hydraulic conductivity for materials subjected to increasing voltages. Interestingly, the decrease in hydraulic conductivity of a cemented sand compared to a clean (i.e., untreated) sand can be as high as one order of magnitude for the highest voltage (4.0 V). In all cases, the results show a higher hydraulic conductivity of loose compared to dense sands because of the more porous packing of the former compared to the latter.

An analysis of the correlation between the unconfined compressive strength and the mass cement content of the tested sands (Fig. 3b) shows that both loose and dense sands benefit from a marked increase in strength

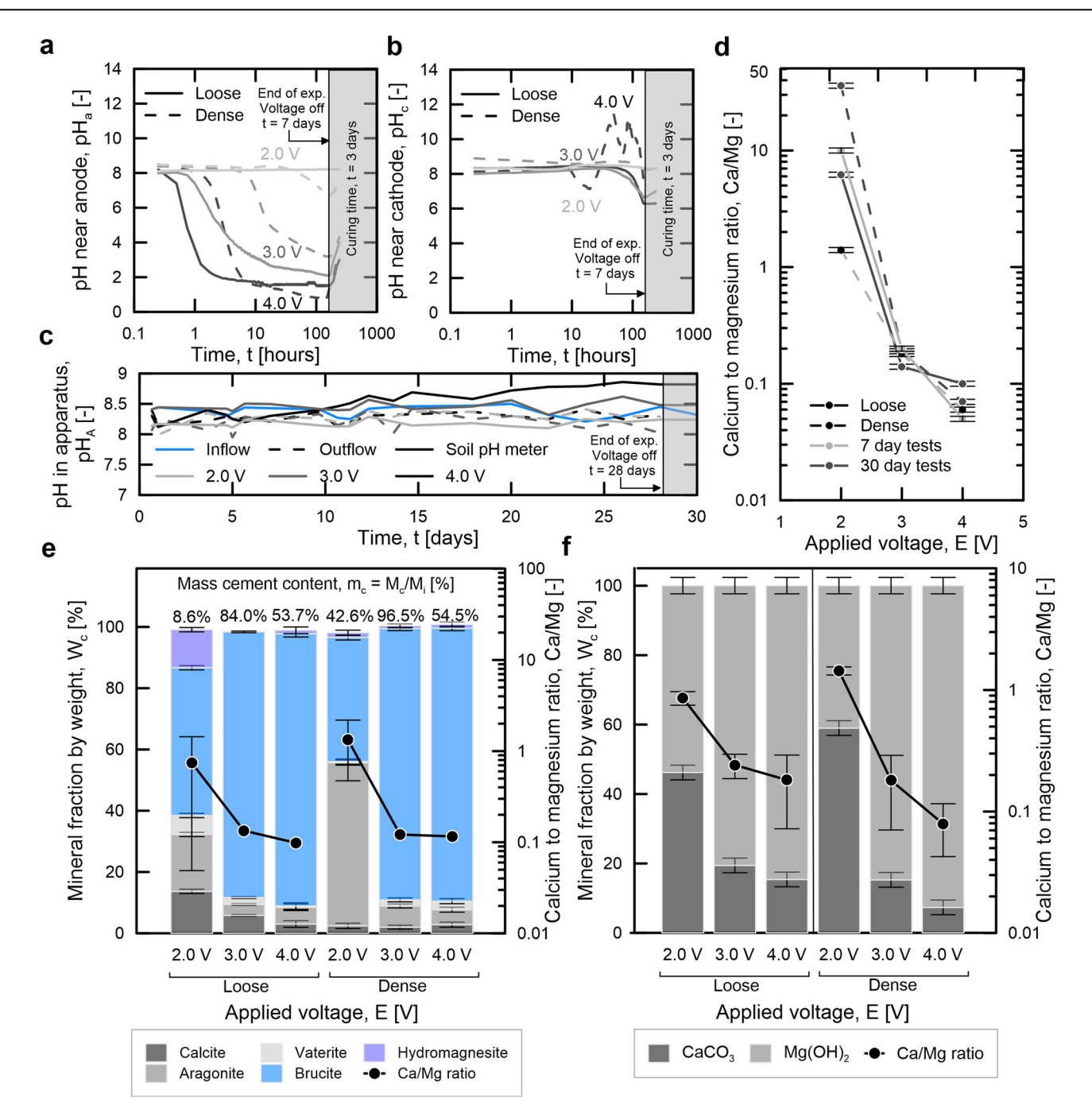


Fig. 2 | Chemical characterization on the environmental parameters and electrodeposited minerals on silica sand. a Evolution of pH over time near the anode for short-term experiments (7 days), measured via a pH meter; **b** Evolution of pH over time near the cathode for short-term experiments (7 days), measured via a pH meter; **c** Evolution of pH over time in the electrochemical cell and at the inlet and outlet of the cell for long-term experiments (28 days), measured via a pH meter; **d** Summary of the elemental ratio of calcium over magnesium (Ca/Mg) obtained for loose and dense sands at different voltages (2.0, 3.0, and 4.0 V) for both short-term

and long-term tests through EDS mapping (error bars indicate standard deviations); **e** Summary of the relative weight of mineral according to Rietveld refinement deriving from XRD analyses of sands (m_c is the mass cement content, with M_c the mass of the cementing calcareous deposits and M_i the mass of the cemented soil; error bars indicate standard deviations); **f** Summary of the relative weight of minerals according to TGA measurements for sands subjected to long-term electrical conditioning (error bars indicate standard deviations).

with the mass cement content. The electrodeposits can yield cemented sands with *UCS* reaching several MPa. In other words, electrodeposition can turn initially cohesionless sands into rocks.

Discussion

Mechanistic analysis of electrodeposition reactions and effects

The results unveil a selectivity of the mineral type, polymorph, proportions, precipitation loci, and intrusion mechanisms achieved by electrodeposition

in marine sands depending on the (1) applied voltage, (2) soil relative density, and (3) electrolyte ionic concentration.

The applied voltage fundamentally influences the process and effects of electrodeposition in sands by triggering different electrochemical reactions that govern the kinetics of mineral precipitations and their penetration in the bulk of the treated materials. An analysis of the applied voltages with respect to a reference electrode (see Supplementary Discussion, Supplementary Figs. 7 and 8, and Supplementary Table 1) indicates that two key

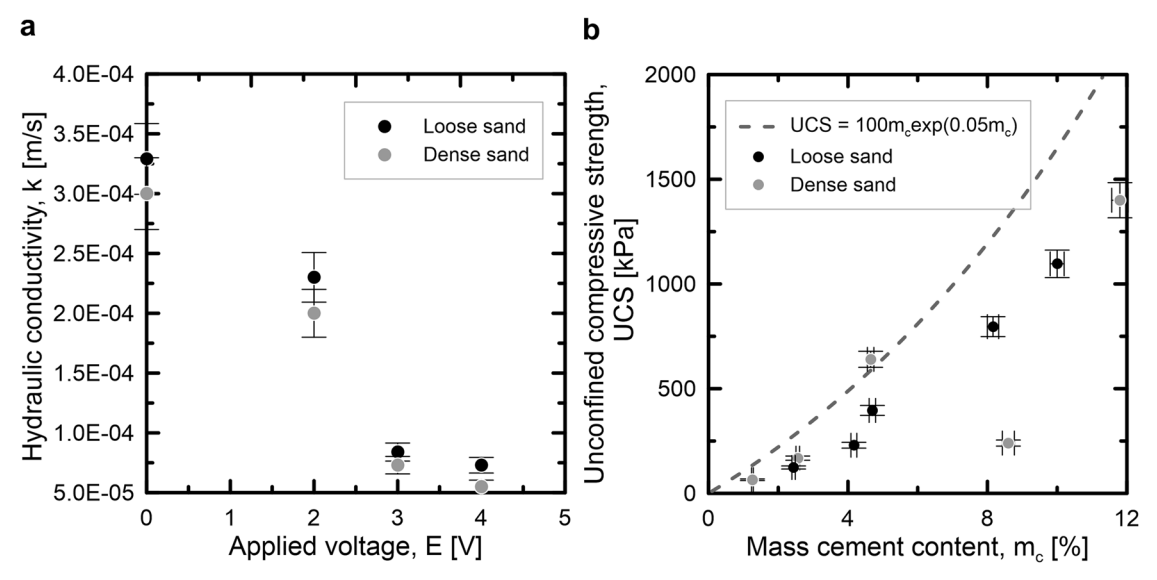


Fig. 3 | Influence of electrodeposition on the bulk hydro-mechanical properties of silica sands. a Variation in hydraulic conductivity as a function of applied voltage level for both loose and dense sands subjected to long-term electrical conditioning; b Variation in unconfined compressive strength against mass cement content for both loose and dense sand (the samples tested refer to long-term electrical

conditioning tests involving the application of 3.0 and 4.0 V; the trendline refers to variations in unconfined compressive strength achieved by microbially induced calcite precipitation in a myriad of coarse-grained soils, including sands³⁸). Error bars indicate standard deviations.

redox reactions govern the electrodeposition in sands: the oxygen reduction reaction (ORR) and the water reduction reaction (WRR). The identification of the reaction regimes corresponding to the application of 2.0, 3.0, and 4.0 V specifically allows identifying the reaction pathways that result in the electrodeposition of $Mg(OH)_2$, $CaCO_3$, and $Mg_5\left(CO_3\right)_4(OH)_2 \cdot 4H_2O$ in the experiments.

At the lower voltage of 2.0 V, which is equivalent to $-0.84~V_{Ag/AgCl}$ or $-0.64~V_{SHE}$, ORR involves OH^- production as follows:

$$O_2 + 2H_2O + 2e^- \rightleftharpoons H_2O_2 + 2OH^- \qquad E^o = -0.146 V_{SHE} | -0.343 V_{Ag/AgCI}$$
(1)

At the higher voltages of 3.0 and 4.0 V, which correspond to $-1.32 \ V_{Ag/AgCl}$ or $-1.13 \ V_{SHE}$ as well as $-1.58 \ V_{Ag/AgCl}$ or $-1.38 \ V_{SHE}$, respectively, WRR shifts selectivity of OH^- production through hydrogen evolution, thereby leading to the formation of hydrogen gas bubbles at the cathode surface. Under neutral and alkaline conditions, hydrogen evolution proceeds as follows:

$$2H_2O + 2e^- \rightleftharpoons H_2(\uparrow) + 2OH^- \qquad E^o = -0.8277 \ V_{SHE}| - 1.0247 \ V_{Ag/AgCl}$$
 (2)

Under acidic solutions, hydrogen evolution proceeds instead as follows:

$$2H^{+} + 2e^{-} \rightleftharpoons H_{2}(\uparrow)$$
 $E^{o} = 0 V_{SHE}| - 0.197 V_{Ag/AgCl}$ (3)

The direct consequence of the generation of OH^- ions in the vicinity of a cathode, whether in either the ORR or WRR regimes, is an increase in the interfacial pH^{17} . Due to this phenomenon, naturally occurring Mg^{2+} ions in seawater will react with the released OH^- ions, leading to the precipitation of insoluble $Mg(OH)_2$ as follows:

$$Mg^{2+} + 2OH^{-} \rightarrow Mg(OH)_{2}(\downarrow)$$
 (4)

In other words, upon the application of electrical stimulations to sands wetted by seawater under ambient conditions, $Mg(OH)_2$ will precipitate initially instead of $CaCO_3$ due to the higher concentration of Mg^{2+} ions

compared to Ca^{2+} ions in seawater. Under these conditions, the mineral formation process is specifically driven by kinetics instead of thermodynamics. Following a decrease in the local pH and concentration of Mg^{2+} ions in solution resulting from the precipitation of $Mg(OH)_2$, two possible outcomes will subsequently occur.

On the one hand, in the ORR regime, $CaCO_3$ will precipitate atop the initial $Mg(OH)_2$ formations due to a favorable local pH that is nonetheless insufficient for continued $Mg(OH)_2$ precipitations. In this context, Ca^{2+} and HCO_3^- ions naturally present in seawater will react with the released OH^- ions, resulting in the precipitation of insoluble $CaCO_3$ as follows:

$$Ca^{2+} + HCO_2^- + OH^- \leftrightarrow H_2O + CaCO_2(\downarrow)$$
 (5)

Alternatively, $CaCO_3$ precipitation will also possibly occur due to the influence of the released OH^- ions on the carbonate equilibrium:

$$CO_2 + H_2O \leftrightarrow H_2CO_3 \leftrightarrow H^+ + HCO_3^- \leftrightarrow H^+ + CO_3^{2-}$$
 (6)

which will lead to a higher concentration of carbonate ions (CO_3^{2-})

$$OH^- + HCO_3^- \to H_2O + CO_3^{2-}$$
 (7)

and the consequent precipitation of insoluble CaCO₃ as follows:

$$Ca^{2+} + CO_3^{2-} \rightarrow CaCO_3(\downarrow)$$
 (8)

On the other hand, in the WRR regime, $Mg(OH)_2$ will continue to precipitate instead of $CaCO_3$ due to a sufficiently high local pH driven by hydrogen evolution. Consistent with results presented here for soils wetted by seawater and studies of electrodeposition in seawater^{21,27,30}, the Ca/Mg ratio will hence decrease with increasing values of the applied voltage. However, as the pH of seawater is typically of 8.2-8.4³¹ under standard conditions but the pH of stability of brucite is of 9.4 under ambient conditions³², brucite will turn into aragonite over time²⁸. Notably, in the WRR regime, the penetration of electrodeposits in the pore network of soils will be facilitated by the formation a hydrogen gas front that pushes the electrodeposits away from the cathode.

In addition to Mg(OH)2 and CaCO3, the results of this work surprisingly support the electrodeposition of $Mg_5(CO_3)_4(OH)_2 \cdot 4H_2O$ in soils wetted by seawater. To the best of our knowledge, the identification of hydromagnesite appears unprecedented in the literature about electrodeposition in seawater^{17,18}, as only $Mg(OH)_2$ and $CaCO_3$ have been traditionally identified. Interestingly, the presence of dissolved silica in the soilwater system considered here may play an important for this evidence, as silica is renowned to play a catalytic role in the development of magnesium bearing carbonates³³. $Mg_5(CO_3)_4(OH)_2 \cdot 4H_2O$ preferentially forms in the ORR regime and in the early stages of WRR regime, characterized by relatively slow kinetics. This evidence, quantitatively supported by the results of Raman spectroscopy and XRD analyses, is attributed to successive pH and salinity fluctuations associated with the alternating formation of $Mg(OH)_2$ and $CaCO_3$ observed in this regime, as opposed to the sustained pH leading to the preferential growth of only $Mg(OH)_2$, which is characteristic of the fully established WRR regime due to hydrogen evolution. Under these conditions, $Mg_5(CO_3)_4(OH)_2 \cdot 4H_2O$ can form due to the local availability of Mg^{2+} , CO_3^- , and OH^- ions in solution, which results in the precipitation of such an hydrated form of magnesium carbonate, $MgCO_3$. The precipitation of $Mg_5(CO_3)_4(OH)_2 \cdot 4H_2O$, instead of MgCO₃, takes place at ambient temperature because it is kinetically favored due to the high hydration character of Mg²⁺ ions in solution³⁴. However, hydromagnesite is a metastable mineral form that will eventually transform (through dehydration and recrystallization) into anhydrous magnesite, either at elevated temperatures or under high CO₂ pressures³⁵. This phenomenon is anticipated to further enhance the strength of electrodeposited sands, as MgCO₃ has better mechanical properties than $Mg_5(CO_3)_4(OH)_2 \cdot 4H_2O$.

Complementary oxidation reactions proceed at the anode, which balance the reduction reactions of water at the cathode. In the ORR, oxygen evolution leads to:

$$H_2O_2 \rightleftharpoons O_2(\uparrow) + 2H^+ + 2e^- \qquad E^o = +0.695V_{SHE}| + 0.498V_{Ag/AgCl}$$
 (9)

In the WRR regime, oxygen evolution develops in alkaline media as follows:

$$4OH^{-} \rightleftharpoons O_{2}(\uparrow) + 2H_{2}O + 4e^{-}$$
 $E^{o} = +0.401 V_{SHE}| + 0.204 V_{Ag/AgCl}$ (10)

whereas in acidic media as follows:

$$2H_2O \rightleftharpoons O_2(\uparrow) + 4H^+ + 4e^- \qquad E^o = +1.229 V_{SHE} | +1.032 V_{Ag/AgCl}$$
 (11)

Higher applied voltage leads to higher production rates of H_2 and OH^- at the cathode and O_2 and OH^+ at the anode, increasing the driving force for OH^+ and OH^- ions to diffuse further away from the electrodes at which they are produced. This phenomenon can result in a crosstalk of ions between the electrodes and neutralization of the OH^- intended to participate in mineral precipitation as follows:

$$H^+ + OH^- \to H_2O \tag{12}$$

In addition to the applied voltage, the soil relative density also influences polymorph selectivity because changes in the relative density of soils affect the available surface area and number of nucleation sites, which are renowned to govern mineral formations^{36,37}. A looser packing provides a constrained number of ample nucleation surfaces and a facilitated frequency of ionic interactions, which lead to smaller and uniformly distributed electrodeposits. In contrast, a denser packing provides more numerous and smaller nucleation surfaces and a hampered frequency of ionic interactions, which involve larger and less uniform electrodeposits. Increasingly tortuous and denser soils, coupled with the influence of low voltages, specifically appear to involve a slow reaction kinetics that results in alternating $Mg(OH)_2$ and $CaCO_3$ formations (with a smaller amount of precipitated $Mg(OH)_2$ compared to looser soils subjected to the same voltages).

The electrolyte ionic concentration also contributes to polymorph selectivity. The pH variations observed in the closed batch experiments are significant and involve a progressive ionic deprivation of seawater that affects the mineral precipitations. In contrast, minimal pH variations and substantial mineral precipitations are observed in the long-term experiments where seawater is periodically recirculated, and the ionic concentrations of calcium and magnesium ions remain approximately constant. This evidence is considered representative of open seawater conditions due to the continuous replenishment of ions through marine currents and biogenic activity.

Implications for coastal erosion mitigation

The results show that electrodeposition changes the structure of marine sands. As the porous structure of sands progressively fills with newly formed electrodeposits, the porosity is reduced while particle contacts increase and are cohesively bonded. As a result, the hydraulic conductivity of marine soils decreases whereas their shearing strength increases.

The variations in hydraulic conductivity and strength achieved with electrodeposition are consistent in magnitude with those of other emerging methods of soil cementation^{38,39}. Compared to such methods, treatments using electrodeposition benefit nonetheless from their avoidance of external fluid injections and their ability to trigger mineral precipitations in porous networks of highly variable sizes. These advantages result from the pervasive action of the electrically mediated charge transport and mineral precipitation pathways leveraged by electrodeposition. Additionally, treatments targeting the electrodeposition of minerals via electricity deriving from renewable energy sources offer the benefit of producing green hydrogen in the WRR regime, which may be collected for valuable purposes. In principle, a downside of electrodeposition in seawater is that it will lead to chlorine production at significant potentials in the WRR regime^{17,40}, which may affect some fish and marine mammals, especially in closed environments²⁴. In practice, the chemistry of seawater favors dominant oxygen production over chlorine, and any chlorine gas will rapidly neutralize with dissolved organic matter in any open environment²⁴. Therefore, treatments using electrodeposition have significant potential to engineer marine soils sustainably.

In summary, the ability to tailor the hydraulic conductivity and strength of marine sands with electrodeposition appears to bear tremendous relevance for coastal erosion mitigation, as these material properties significantly influence erosion patterns, sediment transports and seepage, and the structural stability of coastal and offshore structures.

Conclusions

Motivated by the lack of sustainable and lasting approaches to mitigate coastal erosion worldwide, this study presented an experimental laboratory study on the electrically mediated precipitation of mineral binders in marine sands via the process of electrodeposition. Specifically, by harnessing custom-designed electrochemical cells, this study systematically and mechanistically explored the electrodeposition of calcium- and magnesium-based minerals in silica sand saturated by seawater. For the first time, this work analyzed the influence of the (1) magnitude and duration of the applied voltage, (2) soil relative density, and (3) electrolyte ionic concentration, which are central variables for any applied electrical treatment, treated porous material, and electrolyte solution, respectively.

The results of this work shed light on distinct reaction mechanisms governing the electrodeposition of $CaCO_3$, $Mg(OH)_2$, and $Mg_5(CO_3)_4$ ($OH)_2 \cdot 4H_2O$ in sands saturated by seawater. A transition from oxygen reduction to water reduction particularly occurs between 2.0 and 3.0 V, with marked hydrogen evolution at 4.0 V. During oxygen reduction, hydroxide formation is mass transport limited and results in predominant $CaCO_3$ depositions, mostly in the form of calcite, with companion $Mg_5(CO_3)_4(OH)_2 \cdot 4H_2O$ formations. During water reduction, hydroxide formation is reaction rate limited and favors $Mg(OH)_2$ productions, mostly in the form of brucite. By identifying these two distinct potential regimes, this work highlights that control of the applied electrode potential, with consideration of the soil relative density and electrolyte features, enables

selectivity of the type of precipitated mineral and polymorph, mineral precipitation location, and mineral intrusion mechanism. Therefore, electrodeposition allows achieving variable effects on the structure and properties of electrodeposited sands. These effects are limited in the oxygen reduction reaction regime. In contrast, they are remarkable in the water reduction reaction regime, where hydrogen evolution enables higher mineral production rates by preventing surface film buildup and electrode passivation, as well as the creation of a gas front that pushes electrodeposits in the soil bulk, affecting significant volumes of soils around cathodic interfaces.

This work advances the knowledge of mineral electrodeposition in soils saturated by seawater, underscoring the feasibility of harnessing such a process to protect coastal areas against erosion processes. Additionally, the results of this work enhance the analysis of problems related to sedimentation, biomineralization, and geological carbon sequestration, which are governed by the nucleation and growth of minerals in porous materials.

Methods

Experimental laboratory tests

This study performed an integrated experimental investigation across different spatial scales (e.g., from the macroscale of sand specimens to the microscale of sand particles) and temporal scales (i.e., from 7 to 28 days of electrical conditioning). Specifically, this work performed two classes of electrochemical laboratory experiments in custom-designed electrochemical cells, followed by several qualitative and quantitative characterization methods to address the physical and chemical properties of the electrodeposits, their spatial distribution and features in the porous structure of the treated soils, and their resulting effects on the hydraulic conductivity and shearing strength of such materials.

Short-term batch experiments (lasting 7 days) with no water recirculation were performed to assess the fundamental mechanisms of electro-deposition in soils. Long-term recirculation experiments (lasting 28 days) with periodic water recirculation were performed to simulate electro-deposition under field conditions and explore the interconnected influence of structural changes on the bulk properties of soils. Each short-term and long-term experiment was repeated three times to ensure repeatability. Among the various features that characterize any (1) applied electrical treatment, (2) treated porous material, and (3) electrolyte solution, these experiments allowed to address the following variables that were hypothesized to play a central role for the electrodeposition of minerals in marine sands:

- Magnitude of applied voltage. This variable was chosen due to its prominent influence on the electrodeposition of minerals in seawater 18, which was unchartered for soils saturated by seawater at the time this work was performed. Voltage levels of E=2.0, 3.0, and 4.0 V were selected to address the efficacy and mineral precipitation mechanisms at relatively low, moderate, and high potentials, respectively. These voltage values also correspond to E=-0.839,-1.323, and -1.579 $V_{Ag/AgCI}$, which correspond to development of the sole oxygen reduction reaction, the onset of the water reduction reaction, and the dominant development of the water reduction reaction, respectively (see Supplementary Discussion).
- Duration of applied voltage. This variable was chosen to explore the spatial growth of electrodeposits over time and assess the presence of a "curing time" for such deposits, which is renowned to characterize other methods for soil cementation resorting to carbonate precipitations³⁹. Test durations of t=7 and 28 days were chosen for this purpose.
- Soil relative density. This variable was chosen due to its prominent influence on soil mechanics⁴¹ and the efficacy of other treatments for soil cementation³⁹ through its impact on the contact topology and packing of granular materials, although this evidence was unchartered for soils subjected to electrodeposition at the time this work was performed. Relative densities associated with loose states ($D_r = 25 \pm 5\%$) and dense states ($D_r = 80 \pm 5\%$) were selected for this purpose.

- Analyzing the soil relative density also allowed to indirectly assess the influence of surface density, which is a critical parameter for the formation of minerals³⁶. Surface density refers to the concentration or availability of sites that are suitable for nucleation, where mineral depositions can prosper⁴¹. Higher surface densities generally translate to a greater number of active sites available for deposition, while lower surface densities indicate a fewer number of available active sites for deposition³⁷.
- Electrolyte ionic concentration. This variable was again chosen based on its prominent influence on the electrodeposition of minerals in seawater¹⁸, although this evidence was unchartered for soils subjected to electrodeposition at the time this work was performed. This variable was indirectly assessed by developing short- and long-term electrical conditioning experiments without or with a periodic replenishment of seawater, respectively. This approach ensured a variable (i.e., decreasing) and quasi-constant (i.e., stable) ionic concentration of seawater during electrodeposition, given that its underlying reactions consume key ions over time if no mass transfer with a source of fresh seawater takes place.

The experimental protocol underpinning the developed electrochemical experiments was as follows. Initially, the sand was compacted in the relevant electrochemical cell to achieve the desired relative density through the pluviation method⁴². Next, the compacted sand was slowly saturated with seawater, by injecting such a fluid at minimal velocity from hose connector located at the bottom of the electrochemical cells to prevent the formation of air bubbles and prevent any noteworthy soil disturbance, which would have otherwise affected the relative density. Then, the sand was allowed to rest for 1 h while ensuring that it achieved full saturation. Afterward, voltage was applied to the electrochemical cell while keeping drainage lines (i.e., the hoses) closed. After the electrochemical conditioning, the lid atop the system was removed and the bottom hose was open to allow for desaturation for 72 h to facilitate the subsequent sample extraction process. Once extracted, the samples were thoroughly washed with deionized water to eliminate any excess sodium chloride (NaCl) and eventually dried for characterization or testing. The same experimental procedure characterized the short- and long-term experiments, at the exception that seawater was recirculated (i.e., flushed out from the top hose) using the peristaltic pump over a period of 8 h to ensure approximately constant pH conditions during each long-term experiment. In the longterm experiments, pH measurements were continuously taken not only inside the cell as in the short-term experiments, but also at the inlet and outlet of seawater flow.

Tested materials

The tested material in this study was F35 sand—a coarse, rounded silica sand composed of over 99% ${\rm SiO_2}$ quarried at Ottawa, Illinois purchased from U.S. Silica. Supplementary Fig. 9 shows the particle size distribution obtained via a sieve analysis as well as optical microscopy and scanning electron microscopy (SEM) images to illustrate qualitative features of the tested material. Supplementary Table 2 summarizes further details of the properties of the tested material. Silica sand was chosen due to its chemical inertness with respect to acid, bases, oxidation, and reduction owing to the strong silicon-oxygen bond present in its crystal structure⁴³.

The tested sand was saturated with artificial seawater to create an electrolyte solution as comparable as possible to actual seawater 14 . Artificial seawater was prepared by mixing distilled Type 1 ultrapure water (18.2 M ω – cm of resistivity at 25 °C from Millipore Sigma) with a "sea salt" preparation mixture (from Lake Products Company LLC) according to the ASTM D1141-98⁴⁴. This process consisted in the dissolution of 41.953 g of sea salt mixture with enough water to make 1 L of total solution. The salts, once mixed and dissolved, yielded a fluid with a chemical composition of over 99% similarity with natural seawater The pH of the prepared solution was measured and adjusted as necessary with weak bases or acids to ensure similarity with natural conditions (i.e., pH = 8.2–8.4 31).

Experimental apparatuses

For this study, two classes of custom-designed tempered glass electrochemical cells of different volume capacities were employed (Supplementary Fig. 10): (1) 2-L capacity cells and (2) 500-mL capacity cells. The 2-L liter cell (Supplementary Fig. 10a) is cylindrical with an inner diameter D = 160 mm, an inner height of H = 120 mm, a thickness t = 5 mm, a flanged top of 15 mm, and two hose connectors with an opening of 9 mm located at heights of $H_1 = 20$ mm and $H_2 = 70$ mm. Similarly, the 500 mL cell (Supplementary Fig. 10b) is cylindrical with an inner diameter D=85mm, an inner height of H = 100 mm, a thickness t = 5 mm, a flanged top of 15 mm, and two serrated hose connectors with an opening of 9 mm located at heights of $H_1 = 20$ mm and $H_2 = 70$ mm. Depending on the experiments, the hose connectors in the cells were used to saturate the tested material with the chosen electrolyte solution and/or to run hydraulic conductivity measurements with an Intlab peristaltic pump. This pump provided a precise liquid dosing of 30 ml/min within the equipment admissible flowrates of 5–50 mL/min, with an accuracy of ± 1 mL/min.

Alongside the developed glass cells, Teflon lids with O-rings were used to seal the cells and ensure a closed environment limiting evaporation and chemical reactions with the atmosphere. The lids of both cells incorporated holes to host the anode, the cathode, two pH meters, and one gas outlet, ensuring optimal monitoring of the environmental conditions in the cells. The cell and lid materials were chosen given their low electrical conductivity and low chemical reactivity to prevent any external contamination into the testing chamber.

The electrode materials were selected to ensure ideal conditions for studying electrodeposition. For the anode material, a platinum rod (with a diameter $D_a=0.78$ mm, a total length of $L_a=100$ mm, and an embedded length of $L_a^* = 70$ and 45 mm in the batch and recirculation experiments, respectively) was chosen to prevent oxidation and ensure a highly controlled flow of electricity. For the cathode material, a steel 316 rod ($D_c = 2.0$ mm, $L_c = 100$ mm, and $L_c^* = 70$ mm for the batch tests; $D_c = 3.0$ mm, $L_c = 100$ mm, and $L_c^* = 45$ mm for the recirculation tests) was chosen for its widespread use in practice. Different electrode embedment lengths were used in the batch and recirculation tests to ensure equivalent current density. All electrochemical measurements gathered in the core electrochemical experiments of this work used a Tektronix Keithley Series 2280 S High Precision Bech Power supply that allowed the measurement of voltage and current. Companion electrochemical measurements gathered in complementary electrochemical experiments employed a Biologic SP 150e potentiostat equipped with electrochemical impedance spectroscopy and the setup detailed elsewhere¹⁷.

Two pH meters (Hanna Instruments soils pH meter HI2002) with an accuracy of $pH=\pm0.01$ were utilized to measure pH at 1.5 cm from each electrode. A calibration of these instruments was performed with buffer solutions of pH=4.01,7.01, and 10.01 from Hanna Instruments.

Supplementary Figs. 10c and 10d shows the experimental set-up for the short-term and long-term electrical conditioning experiments, respectively.

Physical, chemical, hydraulic, and mechanical characterization

Each physical, chemical, hydraulic, and mechanical characterization of the results was repeated at least three times to ensure representativeness and reliability of the data. Errors bars are presented wherever relevant and applicable to show the variability in the obtained results.

Scanning electron microscopy (SEM) was employed to qualitatively study the microscopic features of the minerals and their spatial distribution in the porous network of the sand (Fig. 1a, b, d). SEM analyses employed a Quanta 650 F microscope at an accelerating voltage of 20 kV. Before subjecting to a scanning electron microscope, the electrodeposits were coated with gold (Au) in a 20 nm thickness using a Denton's Desk IV deposition system. The results encompass different scales: the particle scale, showcasing whole sand particles; the interface scale, revealing the contacts between sand and mineral particles; and the mineral scale, focusing on the electrodeposits.

Energy dispersive X-ray spectroscopy (EDS) was employed to qualitatively assess the elemental composition of the materials and create elemental maps (Supplementary Fig. 4). This technique facilitated the identification of electrodeposited minerals and the detection of possible impurities caused by oxidation reactions of the electrodes. Yet, EDS elucidated the analysis of the spatial distribution of elements, thereby providing valuable insights into the microscopic behavior of the material and the mineral intrusion mechanisms. Although it is acknowledged that EDS cannot provide data representative of the three-dimensionality of the precipitation patterns in the tested sands, repeatability analyses confirmed the high consistency in the obtained data, which were also qualitatively in agreement with X-ray diffraction (XRD) and thermogravimetric analyses data (TGA). As XRD and TGA analyses were performed on randomly selected mineral samples from the tested soils and inherently provide representative data of the three-dimensionality of the precipitations, the consistency between all these results provides strong evidence of the soundness of the developed analyses and interpretations.

Raman spectroscopy was carried out using a custom-built, confocal micro-Raman spectrometer with a 300 mW, 458-nm excitation laser (Melles Griot 85-BLS-601). The system was built around an Olympus-BX optical microscope, 0.3-meter spectrograph (Andor Shamrock 303i), and Newton DU970 EMCCD camera from Andor Technology. Neutral density filters were added to reduce the laser power to ~10 mW at the sample. The excitation laser was focused to ~1-2 µm spot size through a 100x objective (Mitutoyo M Plan Apo SL100x) with 13.0 mm working distance and a 0.55 numerical aperture. Spectra were collected from 0-4000 cm⁻¹ Raman shift with an acquisition time of 3 seconds, averaged over 10 acquisitions. The Raman spectra are shown alongside reference spectra at low and high wavenumber regions, enabling a precise identification of calcium- and magnesium-based minerals (Fig. 1c). Supplementary Fig. 1 identifies the characteristic peaks of the studied substances for detailed reference, representing a quantitative and complementary piece of evidence in support of the analysis of the obtained results.

Image processing analyses were used to examine the macroscopic features of the electrodeposited sand, with a focus on the volume affected by electrodeposits (Fig. 1e, f, and Supplementary Fig. 2). The volume calculations were performed analytically through the open-source code Fiji ImageJ⁴⁵. The volume calculations were addressed in three key steps. First, any original image was digitalized. Second, such an image was binarized into two colors (i.e., black and white) to better classify the area of the analyzed view. Such area (A_s) was calculated by the software, and subsequently it was converted into an equivalent cylindrical shape. For this process, the height of the equivalent cylinder was assumed to be the length of the electrode (i.e., $L_c = 100$ mm), and the equivalent diameter, D_{eq} , was calculated as follows:

$$D_{eq} = \frac{A_s}{L_c} [\text{mm}]$$

Finally, based on the geometrization of the irregular volume of electrodeposited sand into an equivalent cylinder, the cemented soil volume (V_e) was calculated without taking in account the volume of the used electrode.

$$V_e = \frac{1}{4} \left(D_{eq} - D_c \right)^2 L_c [\text{mm}^3]$$

XRD analyses were employed to quantitatively assess the composition of the crystal structure and phase composition of electrodeposited minerals, allowing for an accurate detection of polymorphs (Fig. 2e and Supplementary Fig. 5). XRD was performed on samples of electrodeposited sand collected near the cathode for all combinations of voltage levels, relative densities, and test durations. XRD analyses on samples indicated a mineral content ranging from 8.6% up to 96.5%. Powder XRD patterns were collected at room temperature on a STOE-STADI-P powder diffractometer equipped with an asymmetrically curved Germanium monochromator

(CuKa1 radiation, λ = 1.54056 Å) and one-dimensional silicon strip detector (MYTHEN2 1 K from DECTRIS) to identify the crystalline phases of the deposits. The line-focused Cu X-ray tube was operated at 40 kV and 40 mA. The fine powder deposits were packed in an 8 mm metallic mask and sandwiched between two polyimide layers of tape. Intensity data from diffraction angles of 15° to 75° (2 θ) were collected for 1 h per sample. The instrument was calibrated against a NIST Silicon standard (640d) before the measurement. Phase identification was made by Rietveld refinements using the Profex analysis software All the reference spectra were used from the Crystallography Open Database (COD). Specifically, COD 9016706, COD9000229, COD 9015898, COD 9002348, and COD 9007620 spectra were used, corresponding to calcite, aragonite, vaterite, brucite, and hydromagnesite, respectively. The spectrum for quartz was also gathered from The American Mineralogist Crystal Structure Database (AMCSD) and plotted for reference with the label AMCSD 0012866.

TGA was performed to quantitatively assess the mass and composition of electrodeposited minerals (Supplementary Fig. 6). For these experiments, the samples were first grinded into a fine powder (i.e., $<4 \mu m$) using a mortar and pestle and eventually subjected to the analyses. These analyses used a Netzsch STA 449 F3 Jupiter Simultaneous Thermal Analysis instrument purging nitrogen at 50 mL/min. 50 mg of the electrodeposits were placed in a 0.35 ml crucible made of Al_2O_3 with a weight of 200 mg. TGA results were calculated based on the mass loss at different stages of heating. A heating rate of 10 °C/min was used over a temperature range of 40–1000 °C. The weight loss between 200–500 °C was associated with the destruction of OH^- bonds, which are associated with magnesium hydroxide. The weight loss between 500–900 °C was associated with the release of CO₂, which is associated with calcium carbonate. The weights at 200 °C (M_{200}) and 500 °C (M_{500}) were determined from the TGA curves. The difference between the weights in the 200–500 °C range ($\Delta M_{200-500}$ °C = $M_{500} - M_{200}$) gave the weight of the generated water gas. A conversion factor between the atomic weight of magnesium hydroxide (58.32 g/mol) and that of water (18.02 g/mol) needs to be applied and leads to the calculation of mass of magnesium hydroxide as follows:

$$Mg(OH)_2 = \Delta M_{200-500\,^{\circ}\text{C}} \cdot \frac{MW_{Mg(OH)_2}}{MW_{H_2O}} \cdot 100[\%]$$

Similarly, the weights at 500 °C (M_{500}) and 900 °C (M_{900}) were determined from the TGA curves. The difference between the weights in the 500–900 °C range ($\Delta M_{500-900}$ °C = M_{900} – M_{500}) gave the weight of the generated carbon dioxide gas. A conversion factor between the atomic weight of carbon dioxide (44.01 g/mol) and that of calcium carbonate (100.09 g/mol) needs to be applied and leads to the calculation of mass of calcium carbonate as follows:

$$CaCO_3[\%] = \Delta M_{500-900^{\circ}\text{C}} \cdot \frac{MW_{CaCO_3}}{MW_{CO_3}} \cdot 100[\%]$$

The evaluation of mineral mass content was performed through acid washing tests 47 . These tests involved a 5 \pm 0.1 g of sample mixed with 20 mL of a 1 M solution of hydrochloric acid (*HCl*) to dissolve electrodeposits. The remaining solution and insoluble solid was washed with Type 1 ultrapure distilled water on a Fisherbrand P4 grade filter paper for 10 min. The mass cement content was calculated as follows:

$$m_c = 100 - \frac{M_w}{M_i} \cdot 100 = \frac{M_c}{M_i} [\%]$$

where M_w is the mass of the sample post acid wash, M_i is the original mass of the electrodeposited sand sample, and M_c is the mass of the cementing calcareous electrodeposits. The TGA curves allow for the development of derivative thermogravimetric (DTG) curves, which represent the first derivative of the TGA curve. The DTG curves are particularly valuable to

determine inflection points and key variations in weight for deeper interpretations during analyses.

Constant head permeability tests were performed to measure the hydraulic conductivity of the tested sand before and after electrical conditioning (Fig. 3a). The experiments devoted to assessing the hydraulic conductivity of the tested loose and dense sands not subjected to any electrical conditioning were performed right after the preparation of such materials in the cell, without using such materials for any other purpose due to the possible structural disturbance of the sands subjected to a hydraulic gradient for these tests. The experiments devoted to assessing the hydraulic conductivity of the tested loose and dense sands were performed after the application of the electrical conditioning. In this case, reference was made to the long-term experiments because they yielded materials benefitting from a more substantial cementation, which facilitated the quantification of the considered parameter. These tests followed the procedure prescribed by ASTM D3424-19⁴⁸.

Unconfined compressive strength tests were performed to quantify the strength of electrodeposited sands (Fig. 3b). While other tests, such as flume tests, could be considered more relevant to characterize the erosion resistance of materials, the unconfined compressive strength provides direct and first-order information about the erosion resistance of marine sediments, especially when samples of limited size are available 49-51. These tests were performed on cubic sand samples extracted from the cell after the long-term tests (again to cope at best with the available volume of cemented materials). The tested samples were carefully cut after extraction from the testing cell (i.e., clearly, these sand samples did not include the electrodes inside them but were collected around the electrodes) and had dimensions of 10 mm inside to comply the requirements of a Representative Elementary Volume⁵². In alignment with the requirements provided by ASTM D7012-04⁵³, the dimension of these samples was determined in a way to be sufficiently larger than the average particle size of the cemented soils, thereby providing reliable results. Prior to testing, the electrodeposited sand samples were laid on a gypsum capping to avoid stress concentrations and interconnected ill-conditioning of the results. Unconfined compressive strength tests followed the procedure prescribed by ASTM D7012-04⁵³ and were performed with a MTS model C43.104 mechanical testing apparatus.

Data availability

The quantitative data shown in the figures are publicly available at Zenodo: https://doi.org/10.5281/zenodo.12741685.

Received: 4 May 2024; Accepted: 6 August 2024; Published online: 22 August 2024

References

- Luijendijk, A. et al. The state of the world's beaches. Sci. Rep. 8, 6641 (2018).
- Mentaschi, L., Vousdoukas, M. I., Pekel, J.-F., Voukouvalas, E. & Feyen, L. Global long-term observations of coastal erosion and accretion. Sci. Rep. 8, 12876 (2018).
- Zhang, K., Douglas, B. C. & Leatherman, S. P. Global warming and coastal erosion. Clim. Change 64, 41–58 (2004).
- van Rijn, L. C. Coastal erosion and control. Ocean Coast. Manag. 54, 867–887 (2011).
- Masria, A., Iskander, M. & Negm, A. Coastal protection measures, case study (Mediterranean zone, Egypt). J. Coast. Conserv. 19, 281–294 (2015).
- Dean, R. G. Beach Nourishment: Theory and Practice. vol. 18 (World Scientific, 2002).
- Gracia, A., Rangel-Buitrago, N., Oakley, J. A. & Williams, A. T. Use of ecosystems in coastal erosion management. *Ocean Coast. Manag.* 156, 277–289 (2018).
- Goreau, T. J. & Trench, R. K. Innovative Methods of Marine Ecosystem Restoration. (CRC Press, 2012).

- Fernando, H. J. S., Samarawickrama, S. P., Balasubramanian, S., Hettiarachchi, S. S. L. & Voropayev, S. Effects of porous barriers such as coral reefs on coastal wave propagation. *J. Hydro-Environ. Res.* 1, 187–194 (2008).
- Barbier, E. B. Natural barriers to natural disasters: replanting mangroves after the tsunami. Front. Ecol. Environ. 4, 124–131 (2006).
- 11. Borsje, B. W. et al. How ecological engineering can serve in coastal protection. *Ecol. Eng.* **37**, 113–122 (2011).
- Frankignoulle, M. A complete set of buffer factors for acid/base CO₂ system in seawater. J. Mar. Syst. 5, 111–118 (1994).
- Jiang, L.-Q., Carter, B. R., Feely, R. A., Lauvset, S. K. & Olsen, A. Surface ocean pH and buffer capacity: past, present and future. Sci. Rep. 9, 18624 (2019).
- Kester, D. R., Duedall, I. W., Connors, D. N. & Pytkowicz, R. M. Preparation of artificial seawater. *Limnol. Oceanogr.* 12, 176–179 (1967).
- Anthoni, J. F. The chemical composition of seawater. *Magnesium* 2701, e9062 (2006).
- Hilbertz, W. Electrodeposition of minerals in sea water: experiments and applications. *IEEE J. Ocean. Eng.* 4, 94–113 (1979).
- Devi, N. et al. Mechanistic insights into electrodeposition in seawater at variable electrochemical potentials. *Adv. Sustain. Syst.* 8, 2300446 (2024).
- Carré, C. et al. Electrochemical calcareous deposition in seawater. A review. Environ. Chem. Lett. 18, 1193–1208 (2020).
- Hartt, W. H., Culberson, C. H. & Smith, S. W. Calcareous deposits on metal surfaces in seawater—a critical review. *Corrosion* 40, 609–618 (1984).
- Neville, A. & Morizot, A. P. Calcareous scales formed by cathodic protection—an assessment of characteristics and kinetics. *J. Cryst. Growth* 243, 490–502 (2002).
- 21. Yao, C. et al. Formation of calcareous deposits in the tidal zone and its effect on cathodic protection. *Npj Mater. Degrad.* **7**, 30 (2023).
- Yang, Y., Scantlebury, J. D. & Koroleva, E. V. A study of calcareous deposits on cathodically protected mild steel in artificial seawater. *Metals* 5, 439–456 (2015).
- 23. Goreau, T. J. F. & Prong, P. Biorock electric reefs grow back severely eroded beaches in months. *J. Mar. Sci. Eng.* **5**, 48 (2017).
- Goreau, T. J. Marine electrolysis for building materials and environmental restoration. *Electrolysis*, Ch. 13 (eds Linkov, V. & Kleperis, J) 273–290 (IntechOpen, 2012).
- Abe, M., Fukute, T., Yokota, M. & Sasaki, H. Applicability of electrodeposition as a repairing method for deteriorated marine concrete structures. *Rep. Port Harb. Res. Inst.* 30, 41 (1991).
- Rotta Loria, A. F., Shirole, D., Volpatti, G., Guerini, A. & Zampini, D. Engineering concrete properties and behavior through electrodeposition: a review. *J. Appl. Electrochem.* 53, 193–215 (2023).
- Carré, C. et al. Electrochemical limestone synthesis in seawater binds metal grids and sediments for coastal protection. *Environ. Chem. Lett.* 18, 1685–1692 (2020).
- Zadi, L. et al. Physico-chemical stability evaluation of a sedimentary agglomerates use for the coastal protection. *J. Coast. Conserv.* 27, 12 (2023).
- Ševčík, R., Šašek, P. & Viani, A. Physical and nanomechanical properties of the synthetic anhydrous crystalline CaCO 3 polymorphs: vaterite, aragonite and calcite. *J. Mater. Sci.* 53, 4022–4033 (2018).
- Rousseau, C., Baraud, F., Leleyter, L., Jeannin, M. & Gil, O. Calcareous deposit formed under cathodic protection in the presence of natural marine sediments: A 12 month experiment. *Corros. Sci.* 52, 2206–2218 (2010).
- 31. Marion, G. M. et al. pH of seawater. Mar. Chem. 126, 89-96 (2011).
- Pokrovsky, O. S. & Schott, J. Experimental study of brucite dissolution and precipitation in aqueous solutions: surface speciation and chemical affinity control. *Geochim. Cosmochim. Acta* 68, 31–45 (2004).

- 33. Hobbs, F. W. C. & Xu, H. Magnesite formation through temperature and pH cycling as a proxy for lagoon and playa paleoenvironments. *Geochim. Cosmochim. Acta* **269**. 101–116 (2020).
- Deelman, J. C. Breaking Ostwald's rule. Chem. Erde-Geochem. 61, 224–235 (2001).
- Königsberger, E., Königsberger, L.-C. & Gamsjäger, H. Low-temperature thermodynamic model for the system
 Na2CO3 MgCO3 CaCO3 H2O. Geochim. Cosmochim. Acta
 3105–3119 (1999).
- 36. Godinho, J. R. A., Gerke, K. M., Stack, A. G. & Lee, P. D. The dynamic nature of crystal growth in pores. *Sci. Rep.* **6**, 33086 (2016).
- Bang, J.-H. et al. Specific surface area and particle size of calcium carbonate precipitated by carbon dioxide microbubbles. *Chem. Eng. J.* 198–199, 254–260 (2012).
- Landivar Macias, A. & Rotta Loria, A. F. SANISAND-C*: Simple ANIsotropic constitutive model for SAND with Cementation. *Int. J. Numer. Anal. Methods Geomech.* 47, 2815–2847 (2023).
- Terzis, D. & Laloui, L. A decade of progress and turning points in the understanding of bio-improved soils: a review. *Geomech. Energy Environ.* 19, 100116 (2019).
- Dresp, S., Dionigi, F., Klingenhof, M. & Strasser, P. Direct electrolytic splitting of seawater: opportunities and challenges. ACS Energy Lett. 4, 933–942 (2019).
- 41. Mitchell, J. K. & Soga, K. Fundamentals of Soil Behavior. (Wiley, New York, 2005).
- Vaid, Y. P. & Negussey, D. Preparation of reconstituted sand specimens. Adv. Triaxial Test. Soil Rock ASTM STP 977, 405–417 (1988).
- Greenwood, N. N. & Earnshaw, A. 9 Silicon. in Chemistry of the Elements (Second Edition) 328–366 (Butterworth-Heinemann, Oxford, 1997). https://doi.org/10.1016/B978-0-7506-3365-9. 50015-8.
- 44. American Society for Testing and Materials. *ASTM D1141-98*. *Practice for the Preparation of Substitute Ocean Water*. https://doi.org/10.1520/D1141-98R21 (1998).
- Schindelin, J. et al. Fiji: an open-source platform for biological-image analysis. Nat. Methods 9, 676–682 (2012).
- Doebelin, N. & Kleeberg, R. Profex: a graphical user interface for the Rietveld refinement program BGMN. J. Appl. Crystallogr. 48, 1573–1580 (2015).
- 47. Choi, S.-G., Park, S.-S., Wu, S. & Chu, J. Methods for calcium carbonate content measurement of biocemented soils. *J. Mater. Civ. Eng.* **29**, 06017015 (2017).
- 48. American Society for Testing and Materials. *ASTM D2434-19 Standard Test Method for Permeability of Granular Soils (Constant Head)*. (ASTM international, 2019).
- Thorne, C. R. Field measurements of rates of bank erosion and bank material strength. Eros. Sediment Transp. Meas. 133, 503–512 (1981).
- Kamphuis, J. W. & Hall, K. R. Cohesive material erosion by unidirectional current. J. Hydraul. Eng. 109, 49–61 (1983).
- Skafel, M. G. & Bishop, C. T. Flume experiments on the erosion of till shores by waves. Coast. Eng. 23, 329–348 (1994).
- Al-Raoush, R. & Papadopoulos, A. Representative elementary volume analysis of porous media using X-ray computed tomography. *Powder Technol.* 200, 69–77 (2010).
- American Society for Testing and Materials. ASTM. D7012-04 Standard Test Method for Compressive Strength and Elastic Moduli of Intact Rock Core Specimens under Varying States of Stress and Temperatures. (West Conshohocken, PA, USA., 2004).

Acknowledgements

The authors would like to thank Prof. Jean-François Gaillard, Dr. Nishu Devi, and Dr. Yeong-Man Kwon for their insightful comments on this work. Dr. Yeong-Man Kwon is particularly thanked for contributing to the XRD analyses performed as a part of this study. Dr. Raul Marrero is thanked for his

help with the training on the sample preparation and mechanical testing procedures under unconfined conditions. This work made use of the EPIC facility of Northwestern University's NUANCE Center, which has received support from the SHvNE Resource (NSF ECCS-2025633), the IIN, and Northwestern's MRSEC program (NSF DMR-1720139), of the IMSERC Crystallography facility at Northwestern University, which has received support from the Soft and Hybrid Nanotechnology Experimental (SHyNE) Resource (NSF ECCS-2025633), and Northwestern University, and the Jerome B.Cohen X-Ray Diffraction Facility supported by the MRSEC program of the National Science Foundation (DMR-1720139) at the Materials Research Center of Northwestern University and the Soft and Hybrid Nanotechnology Experimental (SHyNE) Resource (NSF ECCS-1542205.). The seed funding provided by the Center for Engineering Sustainability and Resilience of Northwestern University in support of early developments behind this work is appreciated. This study is part of a broader research program funded by the Army Research Office (Grant No. W911NF2210291), whose financial support is greatly acknowledged.

Author contributions

A.F.R.L. conceived the study idea and with A.L.M. designed the experimental apparatus and procedures. A.L.M. carried out the experiments and data acquisition during cementation. A.L.M., S.D.J., and A.F.R.L. conducted sample characterizations and data reduction. All authors contributed equally to interpreting the data and writing the manuscript.

Competing interests

The authors declare no competing interests.

Additional information

Supplementary information The online version contains supplementary material available at https://doi.org/10.1038/s43247-024-01604-3.

Correspondence and requests for materials should be addressed to Alessandro F. Rotta Loria.

Peer review information Communications Earth & Environment thanks the anonymous reviewers for their contribution to the peer review of this work. Primary Handling Editors: Olusegun Dada and Carolina Ortiz Guerrero. A peer review file is available.

Reprints and permissions information is available at http://www.nature.com/reprints

Publisher's note Springer Nature remains neutral with regard to jurisdictional claims in published maps and institutional affiliations.

Open Access This article is licensed under a Creative Commons Attribution-NonCommercial-NoDerivatives 4.0 International License, which permits any non-commercial use, sharing, distribution and reproduction in any medium or format, as long as you give appropriate credit to the original author(s) and the source, provide a link to the Creative Commons licence, and indicate if you modified the licensed material. You do not have permission under this licence to share adapted material derived from this article or parts of it. The images or other third party material in this article are included in the article's Creative Commons licence, unless indicated otherwise in a credit line to the material. If material is not included in the article's Creative Commons licence and your intended use is not permitted by statutory regulation or exceeds the permitted use, you will need to obtain permission directly from the copyright holder. To view a copy of this licence, visit http://creativecommons.org/licenses/by-nc-nd/4.0/.

© The Author(s) 2024